Multimode Emission in GaN Microdisk Lasers

Monty Drechsler, Luca Sung-min Choi, Farsane Tabataba-Vakili, Felix Nippert, Aris Koulas-Simos, Michael Lorke, Stephan Reitzenstein, Blandine Alloing, Philippe Boucaud, Markus Wagner, et al.

Multimode Emission in GaN Microdisk Lasers

Monty L. Drechsler, Luca Sung-Min Choi, Farsane Tabataba-Vakili, Felix Nippert, Aris Koulas-Simos, Michael Lorke, Stephan Reitzenstein, Blandine Alloing, Philippe Boucaud, Markus R. Wagner, Frank Jahnke

M. L. Drechsler, M. Lorke, F. Jahnke
Institute for Theoretical Physics, University of Bremen, Otto-Hahn-Allee 1, 28359 Bremen, Germany
E-mail: mon_dre@uni-bremen.de
L. S.-M. Choi, F. Nippert, A. Koulas-Simos, S. Reitzenstein
Institute of Solid State Physics, Technische Universität Berlin, Hardenbergstr. 36, 10623 Berlin, Germany
E-mail: luca.choi@physik.tu-berlin.de; felix@physik.tu-berlin.de; aris.koulas-simos@tu-berlin.de; stephan.reitzenstei
berlin.de;
M. R. Wagner
Paul-Drude-Institut für Festkörperelektronik, Leibniz-Institut im Forschungsverbund Berlin e.V., Hausvogteiplatz 5-7, 10117 Berlin, Germany
Institute of Solid State Physics, Technische Universität Berlin, Hardenbergstr. 36, 10623 Berlin, Germany
E-mail: wagner@pdi-berlin.de
F. Tabataba-Vakili
Fakultät für Physik, Munich Quantum Center, and Center for NanoScience (CeNS), Ludwig-Maximilians-Universität München, Geschwister-Scholl-Platz 1, 80539 München, Germany
Munich Center for Quantum Science and Technology (MCQST), Schellingtraße 4, 80799 München, Germany
E-mail: f.tabataba@lmu.de
B. Alloing, P. Boucaud
Université Côte d'Azur, CNRS, CRHEA, rue Bernard Grégory, 06905 Sophia-Antipolis, France
E-mail: blandine.alloing@crhea.cnrs.fr; philippe.boucaud@crhea.cnrs.fr

Keywords: *Microdisk, Gallium-Nitride, Whispering-Gallery, Multimode, Microlasers, Quantum-Optical, Theory*

Quantum well nanolasers usually show single-mode lasing, as gain saturation suppresses emissions in other modes. In contrast, for whispering gallery mode microdisk lasers with GaN quantum wells as active material, we observe above threshold multimode laser emission. This intriguing emission feature is manufested in the fact that several modes simultaneously show the characteristic kink in the input-output curve at the onset of lasing. A quantum theory for nanolasers is used to support our experimental finding and to analyze this behavior in the presence of gain saturation. We identify coupling effects between neighboring modes as the origin of multimode lasing, which initiate photon exchange between modes via population pulsations similar to classical wave-mixing effects. A reduction of this type of mode coupling with increasing mode spacing is demonstrated. Our results can pave the way for multimode application of nanolasers in integrated photonic circuits.

1 Introduction

Microdisk resonators are important building blocks for integrated photonic circuits [1–3]. Due to their large Q-factors they can serve as a platform for coherent light sources [4, 5]. Multimode operation is of particular interest, as it opens up the prospect for communication over multiple channels in a single waveguide [6, 7] as well as sensing applications [8]. Theoretical understanding of multimode operation provides the fundamentals for on-chip mode division multiplexing without a spatial multiplexer. Nanolasers typically have a large free spectral range (FSR) due to their small resonator dimensions, and therefore single-mode lasing usually prevails [9–11]. This is in particular the case for quantum well (QW) lasers, where emission into the modes is provided by a shared gain medium. Under steady-state conditions, stimulated and spontaneous emission need to balance the cavity losses. Above the laser threshold, this leads to gain saturation which favors stimulated emission for one mode with the highest modal gain. The side-mode suppression through gain saturation of the joint active material acts as a mode-coupling effect. Nevertheless, we observe multimode-lasing in GaN-based whispering gallery mode (WGM) microdisk lasers with a large FSR of several nanometers. Emergence of multimode lasing is well understood in the framework of semiclassical theories. Population pulsations with the beat frequencies between the modes lead to additional mode coupling [12], which results in light scattering between the modes, analogous to non-degenerate four-wave mixing effects.

Laser emission from microdisk resonators has been successfully demonstrated in the visible or ultraviolet spectral range under pulsed optical excitations using III-nitride heterostructures and quantum wells as active regions [13–17]. Various microdisks were obtained using techniques like photo-electrochemical etching, sacrificial layers, underetching, electron-beam lithography, nanosphere lithography in combination with different types of substrates like sapphire or silicon. Single mode [13, 14, 16, 18] or multimode [15, 17, 19–23] lasing was reported in different types of microdisk lasers with various diameters. However, the nature and mechanisms behind multimode lasing and the appropriate theory and modeling to support experimental observations have remained elusive.

In the WGM microdisk lasers studied in this article, several resonator modes appear within the gain bandwidth of a multi-quantum well active medium. Light-scattering effects between the modes as a result of population pulsations compete with gain saturation and lead to multimode stimulated emission. In our samples, a reduced mode volume (estimated as $15 \times (\lambda/n)^3$ following Ref. [24]) together with the elevated Q-factor of about 7000 alter the spontaneous emission into the laser mode in comparison to the total spontaneous emission. In order to address the influence of spontaneous emission and the mode coupling due to wave-mixing effects, we use a quantum optical multimode laser theory. In this article, we show that wave-mixing effects explain the occurrence of multimode lasing also in a quantum optical laser theory. The strength of the wave-mixing effect is discussed in terms of the FSR.

2 Results and Discussion

2.1 Fabrication of III-nitride microdisk lasers

The investigated microlasers consist of mushroom-type microdisk resonators, which were fabricated from a sample grown by metal organic chemical vapor deposition on a Si(111) substrate. The structure is grown on the wurtzite c-axis and consists of a 220 nm AlN buffer layer followed by a 520 nm thick GaN layer and the optically active region. The active region consists of five 3 nm thick $In_{0.1}Ga_{0.9}N$ quantum wells separated by 7 nm thick GaN barriers. The whole structure is terminated by a 20 nm GaN cap layer. **Figure 1**(a) shows a false color scanning electron microscope image of the processed microdisk. The fabrication of the microdisks was achieved using standard cleanroom processing. A SiO_2 hard mask was deposited on the wafer by plasma enhanced chemical vapor deposition. A UV5 positive resist was used to define the pattern of the microdisk resonators by electron-beam lithography and the oxide layer was etched with reactive ion etching using CH_2F_2 and CF_4 gases. The III-nitride layers were subsequently etched by inductively-coupled plasma dry etching using Cl_2 and BCl_3 gases and the remaining SiO_2 was removed. To achieve optical confinement and to avoid leaking of the modes into the silicon, the

substrate was partially underetched using XeF_2 gas leading to a mushroom-type structure with a narrow pedestal as shown in Figure 1(a). Microdisks with diameters from 3 to 6 µm were obtained, in which the WGMs are confined to the periphery of the disks with slightly inclined sidewalls. Additional information on the III-nitride material characterization can be found in the supplementary material of Ref. [23].

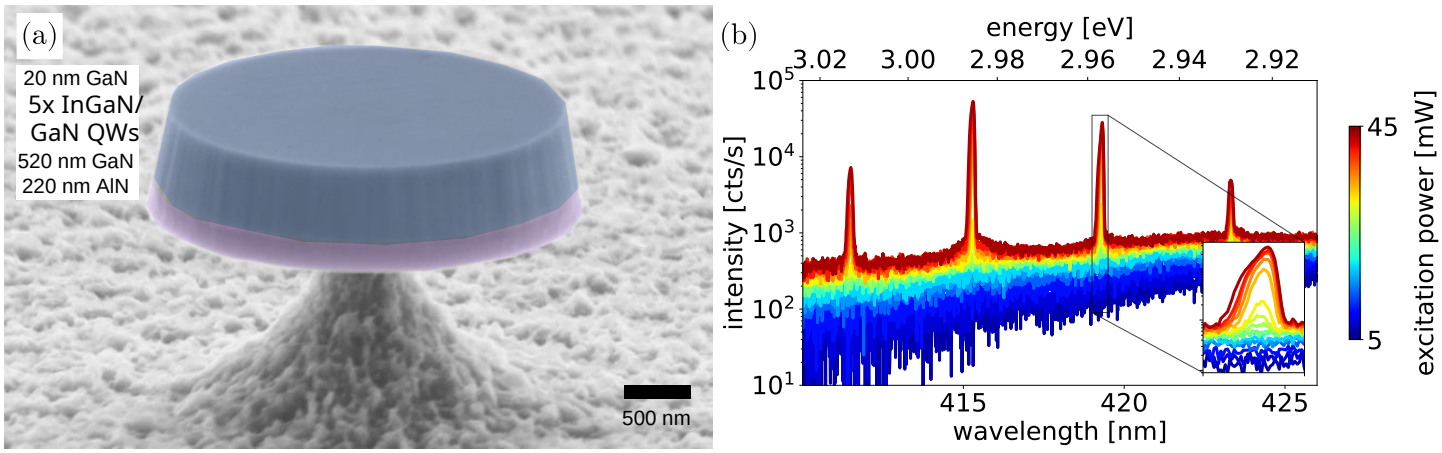

Figure 1: (a) Scanning electron micrograph of a III-nitride microdisk resonator. The III-nitride layers highlighted in false colors are epitaxially grown on a silicon substrate. The layer stacking is indicated on the image. The 220 nm thick AlN layer appears in violet color at the bottom. (b) µ-PL spectra of a microdisk resonator with a diameter of 4 µm at different excitation powers. The zoomed inset shows a mode with a visible secondary feature.

2.2 Experimental optical spectroscopy of the microdisks

The microdisk lasers of different diameter were examined using a micro-photoluminescence (µ-PL) setup. For excitation a frequency-doubled Yb fiber laser, emitting pulses with a frequency of 76 MHz, a wavelength of 515 nm and a pulse duration of approx. 1.5 ps was used. The pulses were frequency doubled again to reach 257 nm and focused onto the sample in backscattering geometry. The collected photoluminescence was guided into a 80 cm focal length Czerny-Turner monochromator with a 1200 mm^{-1} grating providing a 0.03 nm spectral resolution and detected by a liquid-nitrogen cooled CCD. All measurements were performed in a nitrogen atmosphere at room temperature and the pressure was selected to minimize degradation of the sample, presumably caused by laser-induced oxidation or reduced thermal transport [25–27].

Figure 1(b) depicts the power-dependent emission spectra for a microdisk laser with a diameter of 4 µm, where the excitation power ranges between 5 and 45 mW. Four distinct peaks with a FSR splitting of (28.0 ± 0.4) meV clearly arise at (33 ± 5) mW ($\sim$ 100 µJ cm^{-2} per pulse threshold energy) due to the GaN-quantum well emission coupling to the WGMs of the microdisk resonator. The emission of all four modes is present even at the highest excitation power of 45 mW, well above the threshold pump power, thus exhibiting multimode laser operation. Additionally, secondary features are evident next to the resonator's modes at high excitation powers, shown in the zoomed inset in Figure 1(b) and also in the measurements of Ref. [23]. These originate from the lifting of the degeneracy between clock-wise and counter-clockwise modes due to imperfections of the resonator [5, 28, 29]. Lasing was independently verified by second-order photon-autocorrection measurements at 5 K. At room temperature, these measurements are not possible due to low signal to noise ratio.

The experimental results obtained from the 4 µm structure were used as a basis for the development of a theoretical model explaining the underlying mechanism leading to multimode laser operation. From Figure 1(b) Q-factors up to approx. 7000 are deduced.

2.3 Theory-experiment comparison

For the WGM microdisk lasers discussed in this paper, **Figure 2**(a) shows the intensities of the individual modes as well as the total output intensity as a function of the excitation power. The results for the individual mode intensities (solid lines: theory, circles: experiment) reveal a clear kink which indicates the transition to lasing for all four observed modes. Band filling leads to a small shift of the gain maximum. As a result, the weighting of the individual modes changes with increasing excitation power towards higher energies.

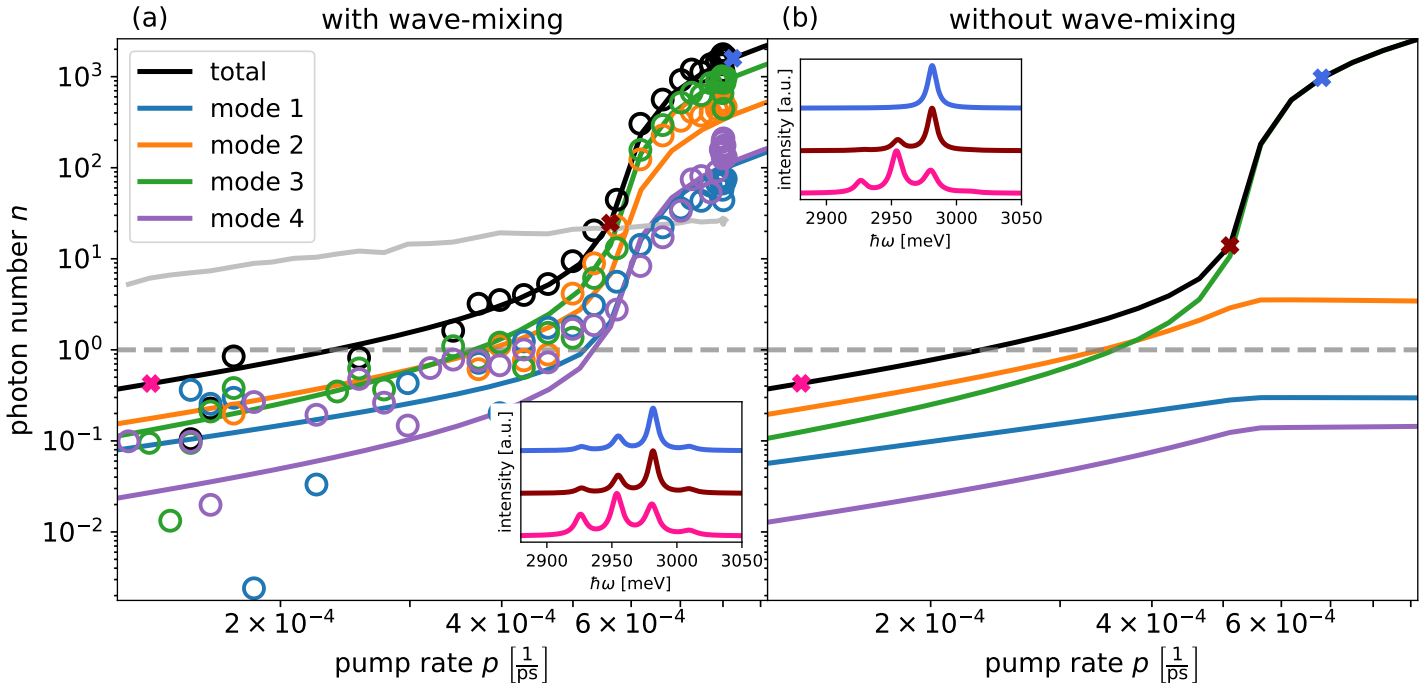

Figure 2: Input-output characteristic of a $In_{0.1}Ga_{0.9}N$ QW nanodisk laser with a diameter of 4 µm. Experimental results for the intensity (open circles) are compared to calculations (solid lines) with (a) and without (b) wave mixing. The experimental intensities and pump rates are scaled with constant factors for direct comparison with the theory. The gray line in (a) shows the background intensity. The insets in (a) and (b) show the calculated emission spectrum of the laser evaluated at the pump rates marked with crosses.

In the following, we investigate the influence of population pulsations and the associated wave-mixing effects on the emissions. For a calculation without wave mixing, Figure 2(b), the total intensity (black solid line) behaves similarly to the previous case. The lasing threshold occurs at smaller pump rates because the main mode (mode with the largest intensity, mode 3) has more photons available and thus higher stimulated emission. For example, a calculated total photon number of 10 is reached for a pump rate of $5.2 \times 10^{-4}\,\mathrm{ps}^{-1}$ with wave mixing and for a pump rate of $4.9 \times 10^{-4}\,\mathrm{ps}^{-1}$ without wave mixing. In the absence of wave mixing, the other modes do not show a transition to lasing, as the corresponding kink is missing.

The behavior of the individual modes in the input-output characteristics is also reflected in the calculated emission spectra, which are provided as insets to Figure 2(a) and (b). When the redistribution of photons due to wave-mixing effect is included, a multimode spectrum is obtained below and above the laser threshold. If the wave-mixing effect is omitted, below threshold pumping leads to an emission spectrum showing several modes. For above threshold pumping, however, the mode with the highest modal gain wins the mode competition and saturates the gain, thereby suppressing emissions to the other modes.

In the wave-mixing process, 2 modes interact with the quantum wells and generate pulsations in the electron population with the difference frequency [12]. As a result, photons can be exchanged between

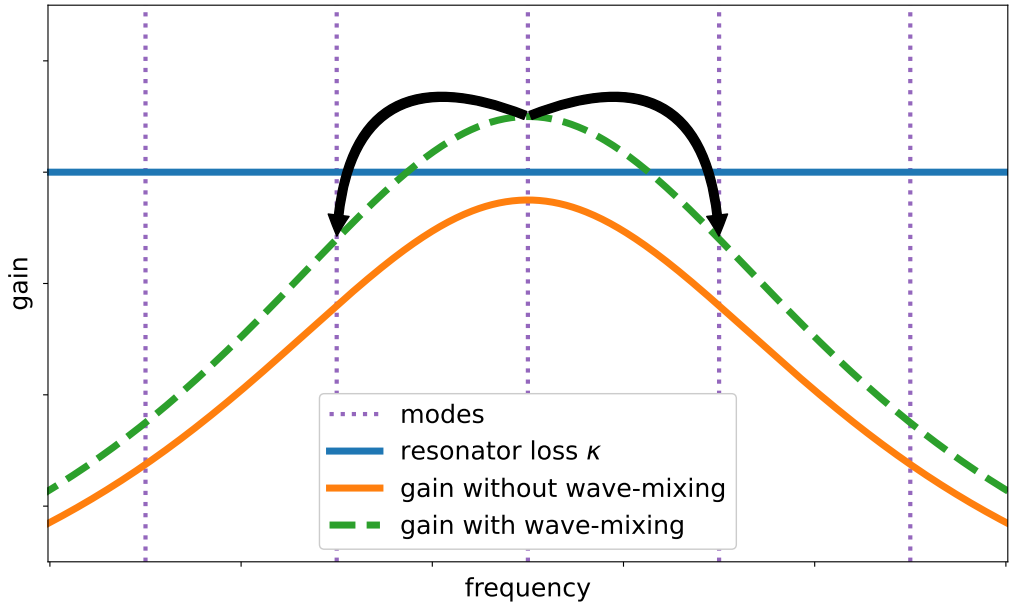

Figure 3: Schematic illustration of the relationship between gain saturation and photon scattering due to wave mixing. The vertical dotted lines mark the spectral positions of the resonator modes. The orange line shows the gain due to stimulated emission and without wave-mixing contributions, which is saturated in such a way that stimulated and spontaneous emission compensate the resonator losses. Due to redistribution of photons by wave mixing, the gain can exceed the resonator losses (green dashed line) as it exhibits additional losses in the total balance.

the modes. The mode with the highest gain scatters photons into other modes, thereby allowing them to pass the laser threshold. This leads to an additional loss channel for the main mode and the gain may exceed the resonator losses for this mode. This increase in gain allows the side modes to pass the laser threshold. **Figure 3** illustrates this phenomenon. Below threshold, a multimode spectrum occurs as spontaneous emission dominates, gain saturation is absent, and a weak wave-mixing process is still present.

2.4 Mode coupling efficiency

The described effects of mode coupling, i.e., the gain saturation of the common active material by the strongest mode and the scattering of photons between the modes, are in themselves generic effects. In addition to the nitride-QW-based WGM microdisk lasers studied here, multimode lasing has been reported in microdisk resonators incorporating arsenide-QWs [30], phosphide-QWs [31] and even perovskites [32]. Multimode lasing was also observed in microdisk resonators with quantum dots as the active medium [28, 33, 34]. In this case, however, multimode operation occurs due to the inhomogeneous broadening of the discrete emitter ensemble, such that each mode only saturates the respective quantum dots in close spectral vicinity. For a large FSR, each laser mode is supported by a separate set of quantum dots and the gain saturation of one mode has no influence on the other modes. We exclude QD-like states due to disorder-induced localization in the used sample. Local fluctuations induced by indium, with a potential in the tens of meV range, are screened under high carrier injection, resulting in delocalized charge carriers at room temperature [35].
For the mode coupling due to photon scattering between the modes, the FSR in relation to the gain bandwidth plays a central role, indirectly also the strength of scattering and dephasing processes. This ultimately makes the processes dependent on the material system and resonator type and lastly dependent on the strength of gain saturation vs. population pulsations.
To investigate the efficiency of mode coupling, we examine the dependence of the emission spectrum on the FSR. **Figure 4** provides the intensities of the individual modes relative to the main mode. The relative intensities decrease exponentially with the FSR (red dashed fits in Figure 4). Thus, multimode

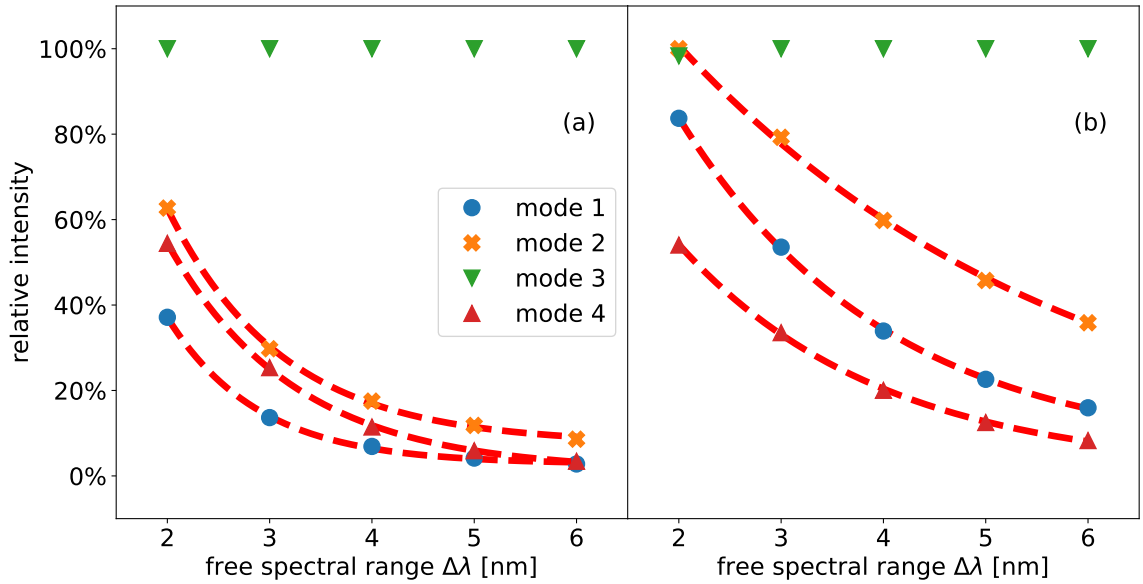

Figure 4: Intensities of the individual modes relative to the intensity of the main mode (mode with the largest intensity) as a function of the FSR, above (a) and below (b) the laser threshold. The red dashed lines are exponential fits.

lasing is less apparent for a larger FSR and photon scattering is less efficient. Below the laser threshold, emission into several modes is supported even with a larger FSR as there is no gain saturation, while the photon scattering remains present albeit at weaker efficiency.
The photon scattering between the modes is represented by processes in which a photon is added into one mode q while being removed from another mode q'. This can be expressed in terms of photon creation and annihilation operators, $b_q^\dagger$ and $b_{q'}$, respectively. The corresponding expectation values $\langle b_q^\dagger b_{q'} \rangle$ with $q \neq q'$ are the off-diagonal photon density matrix elements. These transition amplitudes quantify the efficiency of photon scattering between the modes and are a central part of the used quantum optical multi-mode laser theory. Their calculation is outlined in the **Methods** section. The relative coupling strength (normalized to the square root of the respective photon numbers)

$$\frac{|\langle b_q^\dagger b_{q'} \rangle|}{\sqrt{\langle b_q^\dagger b_q \rangle \langle b_{q'}^\dagger b_{q'} \rangle}} \tag{1}$$

between modes 2 and 3 and the largest pump rate in Figure 2(a) has a value of 15% which emphasizes the magnitude of the process.

3 Conclusion

High Q-factor WGM microdisk resonators with InGaN quantum wells as active material have been used to demonstrate multimode laser operation. A direct analysis of the experimental results with a semiconductor laser theory attributes the simultaneous occurrence of a threshold transition for several laser modes to strong mode coupling effects. Quantum optical semiconductor laser models using a quantization of the optical field play an important role in the analysis of emission properties when the transition from conventional lasers with low Q-factor and low spontaneous emission coupling to nanolasers is performed. While multimode lasing was observed in our present and some previous experiments, quantum optical semiconductor models have focused on treatments with a single laser mode. In this paper we provide the necessary extension to a multi-mode semiconductor theory by including off-diagonal photon density matrix elements. The resulting mode coupling effects turn out to be of strong magnitude and enable multi-mode operation despite the fact that all modes use a common quantum well gain medium and gain saturation is present.

4 Methods

Quantum optical multimode laser theory:
Starting from the Lindblad-von-Neumann equation we derive the equations of motion for relevant expectation values like the mean photon number and first-order photon correlations defining the emission spectrum. The light-matter interaction gives rise to a hierarchy of coupled equations, which is truncated at doublet level of the cluster-expansion approximation [36–38]. We treat interaction of the light field within a two-band model in effective-mass approximation for the $In_{0.1}Ga_{0.9}N$ quantum well (QW) active medium.
For the light-matter-coupling, we consider a Jaynes-Cummings-type interaction with several quantized resonator modes. Our system is described by the Hamiltonian

$$\hat{H} = \sum_k \left(\varepsilon_k^{\mathrm{e}} e_k^\dagger e_k + \varepsilon_k^{\mathrm{h}} h_k^\dagger h_k\right) + \sum_q \hbar\omega_q b_q^\dagger b_q + \sum_{k',q'} \left(g_{k'q'} b_{q'}^\dagger h_{k'} e_{k'} + g_{k'q'}^* b_{q'} e_{k'}^\dagger h_{k'}^\dagger\right), \tag{2}$$

where e_k (h_k) and $e_k^\dagger$ $\left(h_k^\dagger\right)$ are annihilation and creation operators for conduction band electrons (valence band holes), b_q and $b_q^\dagger$ are annihilation and creation operators of photons in the q-th mode, respectively. k represents the state described by wave vector $\vec{k}$ and spin s. The energy of the electrons (holes) in state k is denoted by $\varepsilon_k^{\mathrm{e}}$ $\left(\varepsilon_k^{\mathrm{h}}\right)$, ω_q is the frequency of the q-th cavity mode, and g_{kq} is the light-matter coupling strength between the q-th mode and electrons (holes) in state k. The equations of motion for the photon numbers $n_q = \langle b_q^\dagger b_q\rangle$, the electron occupations $f_k^{\mathrm{e}} = \langle e_k^\dagger e_k\rangle$ and the hole occupations $f_k^{\mathrm{h}} = \langle h_k^\dagger h_k\rangle$ are given by

$$\hbar\frac{\mathrm{d}}{\mathrm{d}t} n_q = 2\sum_k \mathrm{Re}\left\{-\mathrm{i}g_{kq}\left\langle b_q^\dagger h_k e_k\right\rangle\right\} - 2\kappa n_q, \tag{3}$$

$$\hbar\frac{\mathrm{d}}{\mathrm{d}t} f_k^{\mathrm{e/h}} = -2\sum_q \mathrm{Re}\left\{-\mathrm{i}g_{kq}\left\langle b_q^\dagger h_k e_k\right\rangle\right\} - \gamma_{\mathrm{rel}}\left(f_k^{\mathrm{e/h}} - F_k^{\mathrm{e/h}}(T)\right) - \gamma_{\mathrm{r}}\left\langle e_k^\dagger h_k^\dagger h_k e_k\right\rangle + p_k\left(1 - f_k^{\mathrm{e}} - f_k^{\mathrm{h}} + \left\langle e_k^\dagger h_k^\dagger h_k e_k\right\rangle\right). \tag{4}$$

Resonator losses are taken into account with the photon decay rate κ, which is related to the Q-factor of the q-th resonater mode $Q_q = \frac{\hbar\omega_q}{2\kappa}$. The electrons are optically excited high into the conduction band with the pump rate p_k. We use a relaxation time approximation for the scattering of electrons (holes) with rate γ_{rel} towards a Fermi-Dirac distribution $F_k^{\mathrm{e}}(T)$ $\left(F_k^{\mathrm{h}}(T)\right)$ at lattice temperature T. Emission in non-lasing modes is described by loss rate γ_{r}. The corresponding modes are either strongly detuned or have low Q-factors. The occupations n_q and $f_k^{\mathrm{e/h}}$ are driven by the photon-assisted polarization $\langle b_q^\dagger h_k e_k\rangle$, which obeys the differential equation

$$\begin{aligned}\hbar\frac{\mathrm{d}}{\mathrm{d}t}\left\langle b_q^\dagger h_k e_k\right\rangle = {} & \mathrm{i}\sum_{k'} g_{k'q}^*\left\langle e_{k'}^\dagger h_{k'}^\dagger h_k e_k\right\rangle + \mathrm{i}\left(f_k^{\mathrm{e}} + f_k^{\mathrm{h}} - 1\right)\sum_{q'} g_{kq'}^*\left\langle b_q^\dagger b_{q'}\right\rangle \\ & - \left[\mathrm{i}\Delta_{kq} + \kappa + \gamma_{\mathrm{rel}} + \Gamma_{\mathrm{El}} + \Gamma_{\mathrm{Phot}} + \frac{p_k + \gamma_{\mathrm{r}}}{2}\right]\cdot\left\langle b_q^\dagger h_k e_k\right\rangle,\end{aligned} \tag{5}$$

where $\Delta_{kq} = \varepsilon_k^{\mathrm{e}} + \varepsilon_k^{\mathrm{h}} - \hbar\omega_q$ is the detuning of the mode q to the electronic transition at k. Following the cluster-expansion scheme, we explicitly include many-body correlations up to second order in the set of equations used here. On subsequent orders, electron-electron, electron-phonon, and higher-order electron-photon correlations appear, which lead to dephasing contributions in the photon-assisted polarization, described by Eq. (5). As we do not treat these higher-order correlations explicitly, their contributions are added as phenomenological dephasing constants. Here Γ_{El} represents dephasing due to electron-electron and electron-phonon contributions and Γ_{Phot} contains dephasing due to higher-order electron-photon correlations. The $k = k'$ contribution to $\langle e_{k'}^\dagger h_{k'}^\dagger h_k e_k\rangle$ in Eq. (5) describes the spontaneous emission contribution due to recombination of an electron-hole pair with momentum k. Terms

with $k \neq k'$ are polarization-like quantities that account for spontaneous emission processes due to the coupling of different k-states. The dynamics of these processes is given by the equation

$$\hbar\frac{\mathrm{d}}{\mathrm{d}t}\langle e_{k'}^{\dagger}h_{k'}^{\dagger}h_k e_k\rangle = \begin{cases} -\mathrm{i}\sum\limits_q \left[g_{k'q}\Big(f_{k'}^{\mathrm{e}}+f_{k'}^{\mathrm{h}}-1\Big)\langle b_q^{\dagger}h_k e_k\rangle - g_{kq}^{*}\Big(f_k^{\mathrm{e}}+f_k^{\mathrm{h}}-1\Big)\langle b_q e_{k'}^{\dagger}h_{k'}^{\dagger}\rangle\right] \\ -\left[\mathrm{i}\Big(\varepsilon_k^{\mathrm{e}}+\varepsilon_k^{\mathrm{h}}-\varepsilon_{k'}^{\mathrm{e}}-\varepsilon_{k'}^{\mathrm{h}}\Big)+2\gamma_{\mathrm{rel}}+\gamma_{\mathrm{r}}+\dfrac{p_k+p_{k'}}{2}+2\Gamma_{\mathrm{El}}\right]\cdot\langle e_{k'}^{\dagger}h_{k'}^{\dagger}h_k e_k\rangle & \text{for } k\neq k', \\ -2\sum\limits_q \mathrm{Re}\left\{-\mathrm{i}g_{kq}\langle b_q^{\dagger}h_k e_k\rangle\right\}-\gamma_{\mathrm{r}}\langle e_k^{\dagger}h_k^{\dagger}h_k e_k\rangle \\ -2\gamma_{\mathrm{rel}}\cdot\Big(\langle e_k^{\dagger}h_k^{\dagger}h_k e_k\rangle - F_k^{\mathrm{e}}(T)F_k^{\mathrm{h}}(T)\Big)+p_k\Big(1-f_k^{\mathrm{e}}-f_k^{\mathrm{h}}+\langle e_k^{\dagger}h_k^{\dagger}h_k e_k\rangle\Big) & \text{for } k=k'. \end{cases} \tag{6}$$

This expectation value is in turn driven by the photon-assisted polarization $\langle b_q^{\dagger}h_k e_k\rangle$. The second term in Eq. (5) describes the stimulated emission for $q = q'$ and photon scattering for $q \neq q'$. To account for wave mixing we formulate a separate equation:

$$\hbar\frac{\mathrm{d}}{\mathrm{d}t}\langle b_q^{\dagger}b_{q'}\rangle = -\mathrm{i}\sum_k\Big(g_{kq'}\langle b_q^{\dagger}h_k e_k\rangle - g_{kq}^{*}\langle b_{q'}e_k^{\dagger}h_k^{\dagger}\rangle\Big)-\left[\mathrm{i}(\hbar\omega_{q'}-\hbar\omega_q)+2\kappa+2\Gamma_{\mathrm{Phot}}(1-\delta_{q,q'})\right]\langle b_q^{\dagger}b_{q'}\rangle\,. \tag{7}$$

Note that for $q = q'$ the equation for the photon number, Eq. (3), is recovered. For this case, the dephasing contribution Γ_{Phot} is omitted.
The Eqs. (3)-(7) form a closed set of self-consistent laser equations which can be used to determine the input-output characteristics of the nanolasers. Our description goes beyond rate equations, since the polarizations, photon scattering and couplings between different k-states are calculated in a phase sensitive manner (all quantities oscillate with the corresponding transition energy) according to the microscopic interaction processes. An advantage of our approach is that it allows us to study the influence of specific correlation between modes or different k-states.
Furthermore, our theory provides access to the emission spectrum $S(\omega)$ via the first-order photon correlation function $G^{(1)}(t,\tau)$ together with the Wiener-Khinchin theorem [39],

$$S(\omega)=\mathcal{F}\left\{G^{(1)}(t,\tau)\right\}\ \text{with}\ G^{(1)}(t,\tau)=\frac{\hbar}{2\epsilon_0}\sum_{q,q'}\sqrt{\omega_q\omega_{q'}}u_q^{*}(\vec{r}_{\mathrm{D}})u_{q'}(\vec{r}_{\mathrm{D}})\langle b_q^{\dagger}(t)b_{q'}(t+\tau)\rangle\,, \tag{8}$$

where $u_q(\vec{r})$ are the mode functions of the q-th mode and $\vec{r}_{\mathrm{D}}$ denotes the position of the detector. Using the quantum regression theorem [40], we obtain equations of motion for the contributing correlation functions

$$\hbar\frac{\mathrm{d}}{\mathrm{d}\tau}\langle b_q^{\dagger}(t)b_{q'}(t+\tau)\rangle = -\mathrm{i}\sum_k g_{kq'}\langle b_q^{\dagger}(t)h_k e_k(t+\tau)\rangle-(\mathrm{i}\hbar\omega_{q'}+\kappa+\Gamma_{\mathrm{Phot}})\langle b_q^{\dagger}(t)b_{q'}(t+\tau)\rangle\,, \tag{9}$$

$$\begin{aligned}\hbar\frac{\mathrm{d}}{\mathrm{d}\tau}\langle b_q^{\dagger}(t)h_k e_k(t+\tau)\rangle &= \mathrm{i}\left(f_k^{\mathrm{e}}+f_k^{\mathrm{h}}-1\right)\sum_{q'}g_{kq'}^{*}\langle b_q^{\dagger}(t)b_{q'}(t+\tau)\rangle \\ &\quad-\left[\mathrm{i}\Big(\varepsilon_k^{\mathrm{e}}+\varepsilon_k^{\mathrm{h}}\Big)+\Gamma_{\mathrm{El}}+\gamma_{\mathrm{rel}}+\frac{p_k+\gamma_{\mathrm{r}}}{2}\right]\langle b_q^{\dagger}(t)h_k e_k(t+\tau)\rangle\,.\end{aligned} \tag{10}$$

The coupled set of equations (3)-(7) together with (8)-(10) allows us to calculate the emission spectrum of nanolasers in the presence of photon redistribution between different modes. Table 1 shows the parameters used for the calculation.

ε_{g}	$2967\,\mathrm{meV}$
m_{e}	$0.17 \cdot m_0$
m_{h}	$0.74 \cdot m_0$
$\hbar\omega_1$	$2929\,\mathrm{meV}$
$\hbar\omega_2$	$2957\,\mathrm{meV}$
$\hbar\omega_3$	$2985\,\mathrm{meV}$
$\hbar\omega_4$	$3013\,\mathrm{meV}$
g_0	$0.03\,\frac{1}{\mathrm{ps}}$
A	$10^7\,\mathrm{nm}^2$
γ_{rel}	$10\,\frac{1}{\mathrm{ps}}$
T	$50\,\mathrm{K}$
γ_{r}	$0.055\,\frac{1}{\mathrm{ps}}$
κ	$0.373\,\frac{1}{\mathrm{ps}}$
Γ_{Phot}	$7\,\frac{1}{\mathrm{ps}}$
Γ_{El}	$10\,\frac{1}{\mathrm{ps}}$

Table 1: Set of parameters for modeling a $In_{0.1}Ga_{0.9}N$ QW nanodisk laser. m_0 denotes the mass of an electron. The effective masses are determined from [41].

Acknowledgements
M.L.D., L.S.-M.C., and F.T.-V. contributed equally to this work. The Bremen group acknowledges financial support from the Deutsche Forschungsgemeinschaft (DFG project JA619/18-1) and a grant for CPU time at the HLRN (Berlin/Göttingen). The microdisk fabrication was partly supported by the French RENATECH network as well as by the French Agence Nationale de la Recherche (ANR) under MILAGAN convention (No. ANR-17-CE08-0043-02) and Labex GANEX (Grant No. 314 ANR-11-LABX-0014). Support from the Comb-on-GaN convention of Labex GANEX is also acknowledged. A.K-S. and S.R. acknowledge financial support from the DFG via project Re2974/21-1.

Conflict of Interest
The authors declare no conflict of interest.

Data Availability Statement
The data that support the findings of this study are available from the cor-responding author upon reasonable request.

References

[1] G. Roelkens, L. Liu, D. Liang, R. Jones, A. Fang, B. Koch, J. Bowers, *Laser & Photonics Reviews* **2010**, *4*, 6 751–779.

[2] N. Kryzhanovskaya, A. Zhukov, E. Moiseev, M. Maximov, *Journal of Physics D: Applied Physics* **2021**, *54*, 45 453001.

[3] S. Rodt, S. Reitzenstein, *APL Photonics* **2021**, *6*, 1 010901.

[4] X. Jiang, C. Zou, L. Wang, Q. Gong, Y. Xiao, *Laser & Photonics Reviews* **2015**, *10*, 1 40–61.

[5] L. He, Ş. K. Özdemir, L. Yang, *Laser & amp; Photonics Reviews* **2012**, *7*, 1 60–82.

[6] S. J. Choi, K. Djordjev, S. J. Choi, P. Dapkus, *IEEE Photonics Technology Letters* **2003**, *15*, 10 1330–1332.

[7] D. Gostimirovic, W. N. Ye, *Optics Letters* **2021**, *46*, 2 388.

[8] T. Reynolds, N. Riesen, A. Meldrum, X. Fan, J. M. M. Hall, T. M. Monro, A. François, *Laser & Photonics Reviews* **2017**, *11*, 2.

[9] W. W. Chow, S. Reitzenstein, *Applied Physics Reviews* **2018**, *5*, 4.

[10] S. Kreinberg, K. Laiho, F. Lohof, W. E. Hayenga, P. Holewa, C. Gies, M. Khajavikhan, S. Reitzenstein, *Laser & Photonics Reviews* **2020**, *14*, 12 2000065, number: 12.

[11] A. Koulas-Simos, J. Buchgeister, M. L. Drechsler, T. Zhang, K. Laiho, G. Sinatkas, J. Xu, F. Lohof, Q. Kan, R. K. Zhang, F. Jahnke, C. Gies, W. W. Chow, C.-Z. Ning, S. Reitzenstein, *Laser & Photonics Reviews* **2022**, *16*, 9.

[12] M. Sargent, M. O. Scully, W. E. Lamb, *Laser Physics*, Addison-Wesley Publishing Company, Advanced Book Program, **1974**.

[13] E. D. Haberer, R. Sharma, C. Meier, A. R. Stonas, S. Nakamura, S. P. DenBaars, E. L. Hu, *Applied Physics Letters* **2004**, *85*, 22 5179.

[14] A. C. Tamboli, E. D. Haberer, R. Sharma, K. H. Lee, S. Nakamura, E. L. Hu, *Nature Photonics* **2006**, *1*, 1 61–64.

[15] H. W. Choi, K. N. Hui, P. T. Lai, P. Chen, X. H. Zhang, S. Tripathy, J. H. Teng, S. J. Chua, *Applied Physics Letters* **2006**, *89*, 21.

[16] D. Simeonov, E. Feltin, H.-J. Bühlmann, T. Zhu, A. Castiglia, M. Mosca, J.-F. Carlin, R. Butté, N. Grandjean, *Applied Physics Letters* **2007**, *90*, 6 061106.

[17] D. Simeonov, E. Feltin, A. Altoukhov, A. Castiglia, J.-F. Carlin, R. Butté, N. Grandjean, *Applied Physics Letters* **2008**, *92*, 17 171102.

[18] I. Aharonovich, A. Woolf, K. J. Russell, T. Zhu, N. Niu, M. J. Kappers, R. A. Oliver, E. L. Hu, *Applied Physics Letters* **2013**, *103*, 2 021112.

[19] X. Zhang, Y. F. Cheung, Y. Zhang, H. W. Choi, *Opt. Lett.* **2014**, *39*, 19 5614.

[20] J. Sellés, C. Brimont, G. Cassabois, P. Valvin, T. Guillet, I. Roland, Y. Zeng, X. Checoury, P. Boucaud, M. Mexis, F. Semond, B. Gayral, *Scientific Reports* **2016**, *6*, 1 21650.

[21] J. Sellés, V. Crepel, I. Roland, M. El Kurdi, X. Checoury, P. Boucaud, M. Mexis, M. Leroux, B. Damilano, S. Rennesson, F. Semond, B. Gayral, C. Brimont, T. Guillet, *Applied Physics Letters* **2016**, *109*, 23 231101.

[22] Y. Li, L. Feng, F. Li, P. Hu, M. Du, X. Su, D. Sun, H. Tang, Q. Li, F. Yun, *ACS Photonics* **2018**, *5*, 11 4259–4264.

[23] F. Tabataba-Vakili, C. Brimont, B. Alloing, B. Damilano, L. Doyennette, T. Guillet, M. El Kurdi, S. Chenot, V. Brändli, E. Frayssinet, J.-Y. Duboz, F. Semond, B. Gayral, P. Boucaud, *Applied Physics Letters* **2020**, *117*, 12 121103, number: 12.

[24] K. Srinivasan, M. Borselli, O. Painter, A. Stintz, S. Krishna, *Opt. Express* **2006**, *14*, 3 1094.

[25] I. Aharonovich, N. Niu, F. Rol, K. J. Russell, A. Woolf, H. A. R. El-Ella, M. J. Kappers, R. A. Oliver, E. L. Hu, *Applied Physics Letters* **2011**, *99*, 11.

[26] I. Rousseau, G. Callsen, G. Jacopin, J.-F. Carlin, R. Butté, N. Grandjean, *Journal of Applied Physics* **2018**, *123*, 11 113103.

[27] J. Chrétien, Q. M. Thai, M. Frauenrath, L. Casiez, A. Chelnokov, V. Reboud, J. M. Hartmann, M. El Kurdi, N. Pauc, V. Calvo, *Applied Physics Letters* **2022**, *120*, 5.

[28] P. Jaffrennou, J. Claudon, M. Bazin, N. S. Malik, S. Reitzenstein, L. Worschech, M. Kamp, A. Forchel, J.-M. Gérard, *Applied Physics Letters* **2010**, *96*, 7 071103.

[29] R. R. Galiev, N. M. Kondratiev, V. E. Lobanov, A. B. Matsko, I. A. Bilenko, *Physical Review Applied* **2021**, *16*, 6.

[30] M. J. Ries, E. I. Chen, N. Holonyak, G. M. Iovino, A. D. Minervini, *Applied Physics Letters* **1996**, *68*, 11 1540–1542.

[31] T. Zhou, K. W. Ng, X. Sun, Z. Zhang, *Nanophotonics* **2020**, *9*, 9 2997–3002.

[32] Q. Zhang, S. T. Ha, X. Liu, T. C. Sum, Q. Xiong, *Nano Letters* **2014**, *14*, 10 5995 – 6001.

[33] P. Michler, A. Kiraz, L. Zhang, C. Becher, E. Hu, A. Imamoglu, *Applied Physics Letters* **2000**, *77*, 2 184.

[34] F. Albert, C. Hopfmann, A. Eberspächer, F. Arnold, M. Emmerling, C. Schneider, S. Höfling, A. Forchel, M. Kamp, J. Wiersig, S. Reitzenstein, *Applied Physics Letters* **2012**, *101*, 2.

[35] A. David, N. G. Young, M. D. Craven, *Physical Review Applied* **2019**, *12*, 4 044059, publisher: American Physical Society.

[36] C. Gies, J. Wiersig, M. Lorke, F. Jahnke, *Physical Review A* **2007**, *75*, 1 013803, number: 1.

[37] S. Ates, C. Gies, S. M. Ulrich, J. Wiersig, S. Reitzenstein, A. Löffler, A. Forchel, F. Jahnke, P. Michler, *Physical Review B* **2008**, *78*, 15 155319, publisher: American Physical Society.

[38] M. Kira, S. W. Koch, *Semiconductor Quantum Optics*, Cambridge University Press, Cambridge, **2011**.

[39] L. Mandel, E. Wolf, *Optical Coherence and Quantum Optics*, Cambridge University Press, Cambridge, **1995**.

[40] H.-P. Breuer, F. Petruccione, *The Theory of Open Quantum Systems*, Oxford University Press, Oxford, **2007**.

[41] M. Goano, E. Bellotti, E. Ghillino, G. Ghione, K. F. Brennan, *Journal of Applied Physics* **2000**, *88*, 11 6467.

Table of Contents

Quantum well nanolasers usually show single-mode lasing. In this paper, multimode laser emission was observed in whispering gallery mode microdisk lasers with GaN quantum wells as active material. The presence of multimode emission despite gain saturation is explained by photon exchange between modes via population pulsations similar to classical wave-mixing effects.

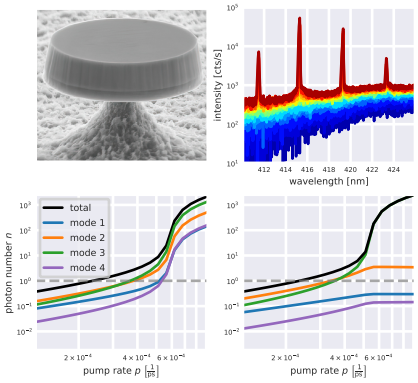

ToC Entry